KNOTS INFLUENCE ON THE BUCKLING LOAD OF TIMBER COLUMNS WITH UNCERTAIN PROPERTIES

Diego A. García[a,b,c], **Mario R. Escalante**[d], **Rubens Sampaio**[e] **and Marta B. Rosales**[a,c]

[a]*Departamento de Ingeniería, Universidad Nacional del Sur, Av. Alem 1253, 8000 Bahía Blanca, Argentina, garciadiego@fio.unam.edu.ar, mrosales@criba.edu.ar.*

[b]*Departamento de Ingeniería Civil, Universidad Nacional de Misiones, Juan Manuel de Rosas 325, 3360 Oberá, Argentina.*

[c]*CONICET, Argentina.*

[d]*Grupo de Métodos Numéricos, FRCU-UTN, Ing. Pereyra 676, 3260 Concepción del Uruguay, Argentina, mrescalante@frcu.utn.edu.ar.*

[e]*Departamento de Ingeniería Mecánica, PUC-Rio, Rua Marquês de São Vicente, 225 22453-900 Rio de Janeiro RJ, Brazil, rsampaio@puc-rio.br.*

Keywords: Timber columns, Knots, Modulus of Elasticity, Random field, Buckling load.

Abstract.

In this work, the static buckling problem of a timber column with geometric and material uncertainties is analyzed. The knots are assumed randomly shaped, sized and located. Also, the Modulus of Elasticity (MOE) is considered as a random field given by a Probability Density Function (PDF) and an exponential correlation function. Two methods are employed to find the PDF of the MOE: the Principle of Maximum Entropy (PME) and a statistical fit using the Kolmogorov-Smirnov (K-S) test, both leading to a Gamma PDF. Meanwhile, the dimensional parameters of the knots are modeled through the Joint Probability Mass Function (JPMF). Experimental data found with bending tests performed on timber beams, classified in strength classes according to the Argentinean standard IRAM 9662-2:2006 are employed to find the PDF parameters of the MOE. On the other hand, experimental data obtained from a visual survey are employed to study the dimensional characteristic of the timber knots and to determine their JPMF. The Nataf transformation and the non-Gaussian Karhunen-Loeve expansion are employed in order to generate and simulate the random field of the MOE and the inverse transform method for the knots parameters. The static buckling load of the timber columns is numerically approximated with the finite element method. Statistics of the response are obtained by means of Monte Carlo Simulations (MCS) with a previous convergence study to determine the acceptable number of realizations. The propagation of the geometric and material uncertainties on the critical load is evaluated through the PDF of the static buckling load. Results obtained by means of MCS are compared with previous numerical outcomes found in limiting cases in order to assess the accuracy of the stochastic model herein presented. Frequently, the presence of knots in sawn timber structures is disregarded, usually due to the lack of data and the availability of an adequate representation. The present approach contributes to attain a more realistic description of the structural components made out of sawn *Eucalyptus grandis* timber.

1 INTRODUCTION

When the tree trunk is converted into structural timber, cuts destroy the interlocking of fibers and knots are created, leaving uncoupled fibers. Due to the specific structure of the trunk and branches, structural timber can be characterized as a composition of clear wood and growth defects. Clear wood is an anisotropic material, but its properties do not change considerably along grains. On the other hand, growth defects such as knots, often related to localized grain deviations, are the main source of the lengthwise variability in the bending strength and stiffness in timber beams. The presence of grain deviations can decrease the MOE in the longitudinal direction. Since knots are unavoidable in structural timber, the effective MOE in the longitudinal direction varies along the main axis of a column. Additionally the reduction of the timber strength and stiffness due to the presence of knots depends on the size of the knots, their type, and their location.

Eucalyptus grandis, which is mainly cultivated in the Argentine Mesopotamian provinces of Entre Rios and Corrientes, is one of the most important renewable species (INTA, 1995). A simple method for visually strength grading sawn timber of these species has been developed by Piter (2003). According to Piter, the presence of pith, or medulla, often associated with other defects as fissures, significantly reduces the strength and the stiffness of this sawn timber. This feature is also considered the most important visual characteristic for strength grading this material by the Argentinean standard IRAM 9662-2 (2006). Other important features taken into account in grading are the knot ratio and the grain deviation (IRAM 9662-2, 2006).

Due to the variability in their mechanical properties, a stochastic approach appears desirable to attain a more realistic structural model and description of its response.

The influence of the knots in the structural behavior of timber beams was first considered by Czmoch (1998). He studied the bending strength in sections with knots and determined the load carrying capacity of timber beams. Czmoch modeled the presence of knots through a Poisson process. Escalante et al. (2012), studied the buckling of *Eucalyptus grandis* wood columns with the finite element methodology and model the lengthwise variation of the MOE as a Normal random process. They also applied Karhunen-Loeve (KL) expansion in order to discretize the random field. Köhler et al. (2007) reported a probabilistic model of timber structures where the MOE was modeled as random variables with a Lognormal PDF, assuming a homogeneous value within a structural element. Then, Köhler (2007), presented a discrete model of the lengthwise variability of the MOE taking into account the presence of timber knots following the model proposed for bending moment capacity reported by Isaksson (1999). In this model, the discrete section transition was assumed to be Poisson distributed. Thus, the length between knots follows an exponential distribution.

The aim of the work is to quantify the influence of the timber knots, the variation in the mechanical properties produced by them, and the lengthwise variability of the MOE in the buckling load of sawn columns of Argentinean *Eucalyptus grandis*. To accomplish this, the PDF of the buckling load was found via Monte Carlo simulations (Rubinstein, 1981). The lengthwise variability of the MOE and of the second moment of area of the column cross section is introduced to account for the knots existence. Frequently, the presence of knots in structures made out of sawn timber is disregarded, maybe due to the lack of data or of an appropriate model. Timber knot parameters are modeled via the joint probability mass function (joint PMF) obtained with experimental data from visual survey of beams of *Eucalyptus grandis* with structural dimensions. In this study timber knots are modeled as holes in the column cross section, hence considered in the second moment of area of the column cross section. This is

due to the grain deviation produced by the knot presence and also because the timber fibers of the trunk have a different orientation that the fibers of the branches. The local reduction of the MOE due to the grain deviation is considered. The lengthwise variability of the MOE, presented in this work, was developed starting from the weak-zone model (Czmoch (1998) and Isaksson (1999)) with modifications in the length of the weak-zone, considered in this work proportional to the greater dimension of the knot. The model herein proposed also takes into account the modification in the column cross section due to the knot presence. The PDF of the MOE was obtained by means of the Principle of Maximum Entropy (Shannon, 1948), and its parameters by means of the maximum likelihood method (MLM) applied to MOE values that were obtained experimentally. In order to measure the fit between the experimental and theoretical PDFs of the MOE and the mass density, the Kolmogorov-Smirnov (K-S) test of fit is used.

Numerical results of pinned-pinned sawn columns of Argentinean *Eucalyptus grandis* are presented and discussed. The PDF and CDF of the buckling load are reported. The influence of the knot modeling is evaluated.

2 PROBLEM STATEMENT

We present the study of the buckling load of a pinned-pinned sawn column of Argentinean *Eucalyptus grandis* with knots, as shown in Figure 1:
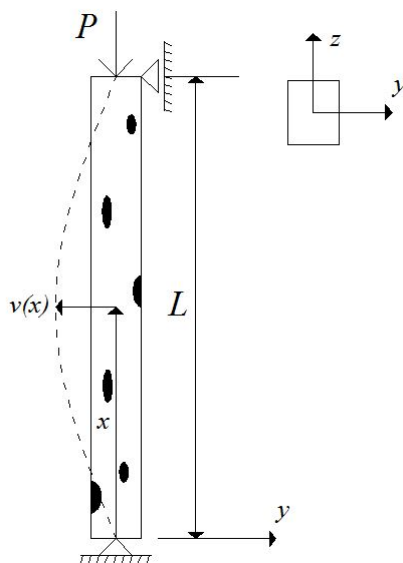

Figure 1: Pinned-pinned sawn column with knots.

According to the Bernoulli-Euler beam theory, the deflection field $v(x)$ and the buckling load p_{cr} of a column of length L are related as follows:

$$\frac{d^2}{dx^2}\left(e(x)i(x)\frac{d^2v(x)}{dx^2}\right) - p_{cr}\frac{d^2}{dx^2}\left(v(x)\right) = 0 \tag{1}$$

where $e(x)$ is the Modulus of Elasticity (MOE); $i(x)$ is the second moment of area of the column cross section with respect to the z axis; $v(x)$ is the transverse displacement and x is the position within the column span.

In the present work, the lengthwise variability of the MOE and of the second moment of area of the column cross section, are introduced due to the presence of timber knots that produce a local reduction of both. Random variables are used and in what follows, these stochastic quantities are denoted by capital letters. The differential equation, Eq. (1), becomes:

$$\frac{d^2}{dx^2}\left(E(x)I(x)\frac{d^2V(x)}{dx^2}\right) - P_{cr}\frac{d^2}{dx^2}\left(V(x)\right) = 0 \tag{2}$$

3 STOCHASTIC FINITE ELEMENT PROCEDURE

Within the variational formulation, a set of admissible functions ψ is prescribed and Eq. (1) can be written as:

$$\int_0^L \left[\frac{d^2}{dx^2}\left(e(x)i(x)\frac{d^2v(x)}{dx^2}\right) - p_{cr}\frac{d^2}{dx^2}\left(v(x)\right)\right]\phi(x)dx = 0 \tag{3}$$

$$\int_0^L e(x)i(x)\frac{d^2v(x)}{dx^2}\frac{d^2\phi(x)}{dx^2}dx - p_{cr}\int_0^L \frac{dv(x)}{dx}\frac{d\phi(x)}{dx}dx =$$

$$\left[e(x)i(x)\frac{d^2v(x)}{dx^2}\frac{d^2\phi(x)}{dx^2} + e(x)i(x)\frac{d^2v(x)}{dx^2}\frac{d\phi(x)}{dx} - p_{cr}\frac{dv(x)}{dx}\phi(x)\right]_0^L \quad \forall \phi(x) \in \psi$$

For the pinned-pinned problem,

$$\psi = \left\{\phi : [0, L] \to \mathbb{R}, \phi \text{ is piecewise } \mathcal{C}^2 \text{ and bounded}, \phi(0) = 0, \phi(L) = 0\right\} \tag{4}$$

and the right hand member is zero giving place to an eigenvalue problem. This formulation together with the boundary conditions conduces to the following form of the variational problem:

$$k(v, \phi) = p_{cr}k^G(v, \phi) \qquad \forall \phi \in \psi \tag{5}$$

where $k(v, \phi)$ and $k^G(v, \phi)$ are the stiffness and geometrical stiffness operators respectively, defined as follows,

$$k(v, \phi) = \int_0^L e(x)i(x)\frac{d^2v(x)}{dx^2}\frac{d^2\phi(x)}{dx^2}dx \qquad k^G(v, \phi) = \int_0^L \frac{dv(x)}{dx}\frac{d\phi(x)}{dx}dx \tag{6}$$

Equation 5 defines a continuous generalized eigenvalue problem. To approximate it numerically, we discretize Eq. 5 using the Galerkin Method, and define a N-dimensional subspace $\psi^N \subset \psi$, where a function $v^N \in \psi^N$. The discrete finite-dimensional variational problem of a buckling column can be now formulated as follows: Find $v^N \in \psi^N$ such that:

$$k(v^N, \phi) = \hat{p}_{cr}k^G(v^N, \phi) \qquad \forall \phi \in \psi^N \tag{7}$$

Applying the standard finite element methodology, see for example Bathe (1996), the variational form Eq. (7) is discretized. Euler-Bernoulli beam elements with two nodes and two degrees of freedom per node (transverse displacement and rotation, respectively) are employed. We consider *Hermitian* shape functions for spatial interpolation of the transverse deflection $v(x)$, in terms of nodal variables.

$$v(x) = n_1(x)v_1 + n_2(x)\theta_1 + n_3(x)v_2 + n_4(x)\theta_2 \tag{8}$$

where

$$n_1(x) = 1 - \frac{3x^2}{L_e{}^2} + \frac{2x^3}{L_e{}^3} \qquad n_3(x) = \frac{3x^2}{L_e{}^2} - \frac{2x^3}{L_e{}^3}$$
$$n_2(x) = x - \frac{2x^2}{L_e} + \frac{x^3}{L_e{}^2} \qquad n_4(x) = -\frac{x^2}{L_e} + \frac{x^3}{L_e{}^2}$$

(9)

where L_e is the element length. The application of $Hermitian$ shape functions and Galerkin's method to Eq.(6) results in the stiffness matrix and the geometrical stiffness matrix of the beam element. The elements of these matrix are respectively:

$$K_{e,ij} = \int_0^{L_e} E(x)I(x)\frac{d^2 n_i(x)}{dx^2}\frac{d^2 n_j(x)}{dx^2}dx \qquad K_{e,ij}^G = \int_0^{L_e} \frac{dn_i(x)}{dx}\frac{dn_j(x)}{dx}dx \qquad (10)$$

where the random quantities $E(x)$ and $I(x)$ represent the lengthwise variability within the column of the MOE and the second moment of area of the column cross section lengthwise variability, respectively. Next, the global matrices can be obtained from the finite element assembling and the buckling load is calculated from the equation

$$K(v^N, \phi) - \hat{p}_{cr} K^G(v^N, \phi) = 0 \qquad (11)$$

where K is the positive-definite global stiffness matrix and K^G is the global geometrical stiffness matrix of elements in compression.

4 MECHANICAL PROPERTIES OF THE MODELS

In this section we present the assumptions and the way in which the mechanical properties that appear in Eq. (2) are represented.

4.1 Random field of the Second Moment of Area: Timber knots shape parameters

In order to simulate the timber knots, we define the joint PMF of the timber knot shape parameters within the timber column cross section, and the probability mass functions of the distance between timber knots and of its length in the direction parallel to the longitudinal axis of the timber column. To find the joint PMF of the knots parameters, experimental data obtained from visual survey of 25 sawn beams of $Eucalyptus\ grandis$ of structural size with 180 timber knots were employed (Piter, 2013). The distance between knots, its dimensions perpendicular and parallel to the longitudinal beam axis, its depth and position within the beam cross section, are the knot features reported in the visual survey.

Considering this visual parameters, the timber knots were classified in four types (Figure 2):

  I - Timber knots with the depth equal to the column width and with vertical position within the column height.

 II - Timber knots with the depth less than the column width and with vertical position within the column height.

III - Timber knots with the depth less than the column width and with vertical position near to the edge of the column cross section.
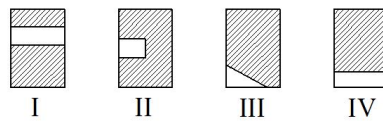
Figure 2: Knots shapes considered in this work.

IV - Timber knots with the depth equal to the column width and with vertical position near to the edge of the column cross section.

Taking into account the parameters which define the position and dimensional characteristic of the timber knots within the column cross section, we define the joint PMF of the three random variables in order to simulate the dimensions of the timber knots and its position within the column cross section:

$$
\begin{aligned}
p_{O,Q,R}(o,q,r) &= p_R(r \mid o,q)p_Q(q \mid o)p_O(o) \\
&= P[R=r \mid O=o, Q=q]P[Q=q \mid O=o]P[O=o] \qquad (12)
\end{aligned}
$$

where the random variables are (see Figure 3):

- O is the position of the knot centroid along the height of the column cross section.

- Q is the knot height (dimension perpendicular to the longitudinal column axis).

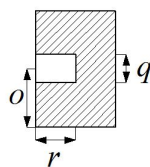- R is the knot depth along the width of the column cross section.

Figure 3: Column cross section with a knot. Variables of the joint probability mass function.

In the type II knots, the timber beams are not cut through the cross section with the knot, after the experimental test to determine its depth r because they become useless to perform other tests. Due to the lack of information about this random variable, the Principle of Maximum Entropy (PME) is applied to obtain the probability distribution of R. The PME states that, subject to known constrains, the joint PMF which best represents the current state of knowledge is the one with largest entropy. The measure of uncertainties of a discrete random variable R is defined by the following expression:

$$
S(p) = -\sum_{i=1}^{n} p_i ln(p_i) \qquad (13)
$$

in which S is the entropy of the random variable and p_i is the probability of the discrete random variable R which assumes n different values. It is possible to demonstrate that the application

of the PME, when the random variable assumes a finite number of values within the interval $[a, b]$ and no further information about the random variable is known, leads to a uniform PMF.

The random variables that define the distance between timber knots and their dimensions in the direction parallel to the column axis are respectively:

- U is the distance between timber knots.

- W is the length of the knot (dimension along to the longitudinal column axis).

and they are defined respectively by the following joint PMF:

$$p_U(u) = P[U = u] \tag{14}$$

$$p_{Q,W}(q, w) = p_W(w \mid q)p_Q(q) = P[W = w \mid Q = q]P[Q = q] \tag{15}$$

The last expression is assumed to simulate the knot shape resulting of the visual survey. This assumption implies that the dimension of the knot in the direction parallel to the longitudinal column axis w is related with its dimension in the direction perpendicular to the axis mentioned q.

In Table 1 the mean values, standard deviations and coefficients of variation of the random variables that represent the characteristics of the timber knots are depicted.

Knot dimension	μ (mm)	σ (mm)	$\delta = \sigma/\mu$
O	61.62	38.77	0.63
Q	23.95	11.46	0.48
R	20.22	11.49	0.57
U	288.62	175.52	0.61
W	40.19	21.36	0.53

Table 1: Statistic values of the timber knots parameters.

4.2 Random field of the Modulus of Elasticity (MOE)

4.2.1 Nataf Transformation

The Nataf transformation is employed in order to generate and simulate the random field of the MOE. It has been introduced by Der Kiureghian and Liu (1986) and allows to build a multidimensional PDF that fits some prescribed marginal distributions and some correlation matrix. Suppose a random vector X has prescribed marginal distributions, say $F_{X_i}(X_i)$, $i = 1, \ldots, M$ and a correlation matrix R. It is possible to transform the components of X into standard Normal random variables ξ_i, $i = 1, \ldots, M$:

$$\xi_i = \Phi^{-1}(F_{X_i}(x_i)) \tag{16}$$

The Nataf transformation assumes that $\Xi = \{\Xi_1, \ldots, \Xi_M\}^T$ is a standard Normal correlated vector whose joint PDF is the multidimensional Normal PDF:

$$\varphi_M(\xi; R_0) = \frac{1}{\sqrt{(2\pi)^M det R_0}} exp\left[-\frac{1}{2}\xi^T R_0^{-1}\xi\right] \tag{17}$$

and R_0 is a correlation matrix (corresponding to the multidimensional Normal PDF) that should be compatible with the prescribed correlation matrix R (corresponding to the random field of the prescribed marginal distribution). From the above equations, one can write:

$$f_X(x_1, \ldots, x_M) = f_\Xi(\xi_1, \ldots, \xi_M) \left| det \mathcal{J}_{\Xi,X} \right| \tag{18}$$

where the Jacobian of the transform is a diagonal matrix with elements $\frac{f_{X_i}(x_i)}{\varphi(\xi_i)}$, $i = 1, \ldots, M$. This leads to the Nataf transformation

$$f_X(x_1, \ldots, x_M) = \prod_{i=1}^{M} \frac{f_{X_i}(x_i)}{\varphi(\xi_i)} \varphi_M(\xi; R_0) \tag{19}$$

The correlation matrix R_0, is computed term by term by solving the following consistency equation for ρ_{ij}:

$$\rho_{ij} = \int_{-\infty}^{\infty} \int_{-\infty}^{\infty} \left(\frac{x_i - \mu_{X_i}}{\sigma_{X_i}} \right) \left(\frac{x_j - \mu_{X_j}}{\sigma_{X_j}} \right) \varphi_2(\xi_i, \xi_j; \rho_{0ij}) d\xi_i d\xi_j \tag{20}$$

where ρ_{ij} and ρ_{0ij} are the non-dimensional correlation matrix elements. For given marginals and correlation coefficient ρ_{ij} of two variables X_i and X_j, the preceding equation can be solved iteratively to find ρ_{0ij}. To avoid such tedious calculations, a set of semi-empirical formulas to the ratio $F = \frac{\rho_{0ij}}{\rho_{ij}}$ have been tabulated for various couples of distributions $(f_{X_i}(x_i), f_{X_j}(x_j))$ in Der Kiureghian and Liu (1986), Ditlevsen and Madsen (1996) and Melchers (1999). In this work $f_{X_i}(x_i)$ and $f_{X_j}(x_j)$ are assumed to be Gamma distributed, hence the value of F is defined as:

$$\begin{aligned} F = \frac{\rho_{0ij}}{\rho_{ij}} &= 1.022 + 0.022\rho_{ij} - 0.012(\delta_i + \delta_j) + 0.001\rho_{ij}^2 + 0.125(\delta_i^2 + \delta_j^2) \\ &- 0.077\rho_{ij}(\delta_i + \delta_j) + 0.014\delta_i\delta_j \end{aligned} \tag{21}$$

where δ_i and δ_j are the coefficients of variation, in our case it has been assumed that $\delta_i = \delta_j$. This assumption is based in the properties of the simulated random field, which is homogeneous and stationary.

4.2.2 Non-Gaussian Karhunen-Loeve Expansion

In addition to the Nataf transformation, in this work the non-Gaussian Karhunen-Loeve Expansion (KLE) is applied in order to simulate the MOE random field. The KLE of the random field of the MOE has the following form:

$$E(x, \theta) = \overline{E}(x) + \sum_{i=1}^{\infty} \sqrt{\lambda_i} \xi_i(\theta) f_i(x) \tag{22}$$

in which λ_i and $f_i(x)$ are the eigenvalues and eigenfunctions of the covariance function $C(x_1, x_2)$, respectively. By definition, $C(x_1, x_2)$ is bounded, symmetric and positive definite. Following the Mercer's Theorem, it has the following spectral decomposition:

$$C(x_1, x_2) = \sum_{i=1}^{\infty} \lambda_i f_i(x_1) f_i(x_2) \tag{23}$$

and its eigenvalues and eigenfunctions are the solution of the homogeneous Fredholm integral equation of the second kind given by

$$\int_D C(x_1, x_2) f_i(x_1) dx_1 = \lambda_i f_i(x_2). \tag{24}$$

The eigenfunctions form a complete orthogonal set satisfying the equation:

$$\int_D f_i(x) f_j(x) dx = \delta_{ij} \tag{25}$$

where δ is the Kronecker-delta function. The parameter ξ_i is a set of uncorrelated random variables which can be expressed as:

$$\xi_i(\theta) = \frac{1}{\sqrt{\lambda_i}} \int_D \left[E(x, \theta) - \overline{E}(x) \right] f_i(x) dx \tag{26}$$

with mean and covariance function given by

$$E[\xi_i(\theta)] = 0 \qquad E[\xi_i(\theta)\xi_j(\theta)] = \delta_{ij} \tag{27}$$

If the random process is Gaussian, then $\xi_i(\theta)$ are zero mean uncorrelated Gaussian variables. Uncorrelated standard Normal variables are independent, so the question of independence does not arise in the KL expansion of a Gaussian random process. In the case of non-Gaussian random variables, uncorrelated and independence are not equivalent. To obtain KLE basis random variables $\xi_i(\theta)$ for a non-Gaussian process, marginal density function should be available.

Following the work of Mulani et al. (2007) the non linear transformation method is applied. The following steps should be carried to obtain KL expansion basis random variables $\xi_i(\theta)$ in the of a non-Gaussian process:

- Calculate the standard deviation and the CDF of the given marginal distribution.

- Calculate the new CDF such that

$$F_{nm}\left(\frac{X_m}{\sigma_m}\right) = F_m(X_m) \tag{28}$$

  where F_m and F_{nm} are the input parameter marginal (m) CDF and the normalized marginal (nm) CDF using the standard deviation, σ_m, respectively. This nonlinear transformation creates random variables with unit variance and the mean of this random variable may be nonzero.

- Generate independent samples of F_{nm} using the CDF inverse technique. Then, calculate the mean of F_{nm}. If the mean is nonzero, subtract this value from generated samples and plot the CDF of F_{nm}^*. F_{nm}^* is the CDF of the basis random variables ξ_i for the non-Gaussian KL expansion.

For the practical implementation, the series were approximated by a finite number of terms, M, giving

$$E(x, \theta) = \overline{E}(x) + \sum_{i=1}^{M} \sqrt{\lambda_i} \xi_i(\theta) f_i(x) \tag{29}$$

4.2.3   Marginal PDF of the MOE

In order to determine the marginal PDF of the MOE, the PME for a continuous random variable is applied, unlike the previous case employed for a discrete random variable. The measure of uncertainties of the continuous random variable X is defined by the following expression

$$S(f_X) = -\int_D f_X(x)ln(f_X(x))dx \tag{30}$$

in which f_X stands for the PDF of X and D is its domain. It is possible to demonstrate that the application of the principle under the constraints of positiveness and bounded second moment, leads to a Gamma PDF.

To find the parameters of the marginal PDF of the MOE, experimental data presented by Piter (2003) are employed. These values were obtained by means of two point load bending tests, performed with 349 sawn beams of Argentinean *Eucalyptus grandis* with structural dimensions. Bending tests were carried out according to the standard UNE-EN408 (1995).

The parameters of the Gamma marginal PDF of the MOE are estimated with the help of the maximum likelihood method (MLM). Then, the Kolmogorov-Smirnov (K-S) test of fit is used, *e.g.* Benjamin and Cornell (1970). The PDF that best fits with the experimental values is the Gamma, in concordance with the PME. The test of fit also was carried out with the Lognormal and Normal PDFs, the first one since Köhler et al. (2007) proposed it to model the MOE and the second PDF as is often employed to represent mechanical properties. The Normal PDF fits the experimental data best. However, the use of this PDF in the model would occasionally leads to negative values of the MOE. Thus, the Gamma and Lognormal PDF seem to be more suitable. The Gamma marginal PDF and CDF of the MOE are respectively:

$$f(x \mid a,b) = \frac{1}{b^a\Gamma(a)}x^{a-1}e^{-\frac{x}{b}} \qquad F(x \mid a,b) = \frac{1}{b^a\Gamma(a)}\int_0^x t^{a-1}e^{-\frac{t}{b}}dt \tag{31}$$

where a and b, denote the shape and scale parameters respectively.

4.2.4   Correlation Function of the MOE Random Field

We assume an exponential correlation function, proposed by Czmoch (1998), based on experimental test carried out in *Pine spruce* timber beams:

$$\rho_{ij} = exp\left(-2\frac{\left|x_c^{(j)} - x_c^{(i)}\right|}{d}\right) \tag{32}$$

where d is the correlation length. In this work, the values considered for the correlation length of the MOE random field, are presented in Table 2.

d_1	d_2	d_∞
0.672 m	1.344 m	$\to \infty$

Table 2: Values of the correlation length d.

In his work, Czmoch (1998) experimentally found that the correlation length of the MOE for *Pine spruce* timber beams, is approximately 1.4 m for the serviceability load level, and around to 0.7 m for a load level close to the load carrying capacity. For the value $d \to \infty$, the random field becomes fully correlated and it can be interpreted as a random variable in the limit (column with homogeneous MOE).

4.2.5 Discretization of the random field

In order to apply the material properties in the beam elements, it is necessary to mesh the random field. The midpoint method consists in associating a random variable, to the centroid of each element of the mesh, and representing the field in each point of the element by this random variable. In this method, a random field $E(x)$ is represented by a set of random variables, defined for random field elements matching with the finite elements, as follows:

$$E_i = E(x_c^{(i)}) \tag{33}$$

where $x_c^{(i)}$ is the location of the centroid of the i-th element. This method is suitable for discretization of a non-Gaussian random field, Czmoch (1998) and Der Kiureghian and Ke (1988).

5 PROBABILISTIC MODELS

5.1 Model 1 (M1)

This model only considers the lengthwise variability of the MOE. The variability in the second moment of area due to the knots presence is not taken into account. The MOE random field $(E(x, \theta))$ is simulated through the Nataf transformation for the values of d shown in the Table 2. Since structural timber columns are composed of clear wood, where the MOE can take higher values, and wood with defects, where the MOE is reduced, we adopted the criteria to determine its PDF parameters with the whole population of experimental values. The parameters of the Gamma marginal PDF of the MOE (Eq. 31) are depicted in Table 3.

Parameters	Values
a	28.727
b	0.440
μ (GPa)	12.639
σ (GPa)	2.358
$\delta = \sigma/\mu$	0.186

Table 3: Parameters of the Gamma marginal PDF of the MOE, M1.

5.2 Model 2 (M2)

This model considers the lengthwise variability of the MOE and in the second moment of area due to the knots presence. The MOE random field $(E(x, \theta))$ is simulated through the Nataf transformation, for the values of d depicted in Table 2, in timber column sections free of the knots presence. In column sections with knots the MOE values are considered uncorrelated random variables which assume values lower than the minimum value of the MOE in the sections without knots. This model is similar to the weak zone model proposed by Isaksson (1999), but unlike this work, it considers the lengthwise variability of the MOE in the sections without knots. In the weak zone model the timber structural component is modeled as a composite of short weak zones connected by longer sections of clear wood.

The MOE values in this model are assigned in function to the knot ratio (K) of each knot or knots clusters as is depicted in Table 4. The PDFs for each knot ratio are the consequence of decomposing the total population of experimental values (Table 3) in the classification presented in Table 4. The knot ratio (K) is calculated as the ratio of the largest dimension of the major knot

or the sum of the individual dimensions of the knots that conform the cluster, in a timber column length equal to its width, measured between tangents to them and parallel to the longitudinal axis of the element, and the transverse dimension of the surface in which they appear. For the knots that are presented on an edge of the cross section the smaller of the two relationships is considered. In this model, the length of the weak zones are proportional to five times the largest

Parameters	$E(x) \to \mathrm{K} = 0$	$E_i \to 0 <\mathrm{K}\le 1/3$	$E_i \to 1/3 <\mathrm{K}\le 2/3$	$E_i \to 2/3 <\mathrm{K}$
a	31.301	42.730	35.370	35.464
b	0.507	0.315	0.364	0.328
μ (GPa)	15.889	13.488	12.879	11.632
σ (GPa)	2.963	2.084	2.148	1.953
$\delta = \sigma/\mu$	0.186	0.160	0.167	0.168

Table 4: Parameters of the Gamma marginal PDF of the MOE, M2.

knot dimension (q, w). This feature was observed in the visual survey of the timber knots and its surrounding fibers. The MOE in each of these zones is constant and randomly assigned.

6   NUMERICAL RESULTS

In this section, numerical results of the buckling load P_{cr} of a pinned- pinned *Eucalyptus grandis* timber column, are reported. The parameters employed in the numerical simulation are the following: column length 2 m and a nominal section of the column 50 mm x 150 mm. These dimensional parameters correspond to timber columns of structural size, which are often used in design practice. The ratio between the length of the column and the lower cross section dimension is equal to 40 ($L/b = 40$). This is equivalent to a slenderness equal to 139 ($\lambda = 139$).

A convergence study of the two probabilistic models is shown in Figure 4, where ns is the number of independent Monte Carlo Simulations (MCS) and $E[P_{cr}]$ is the mean value of the buckling load. The adopted convergence criterion is the following: $|E[P_{cr}^{ns}]| - |E[P_{cr}^{ns-200}]| \le$ 0.1 KN; where $E[P_{cr}^{ns}]$ is the mean value of the buckling load for a number of simulations ns and $E[P_{cr}^{ns-200}]$ is the mean value of the buckling load for a number of simulations $ns - 200$. In this figure, the difference in $E[P_{cr}]$ for the two models can be observed. The M2 show higher values of $E[P_{cr}]$ than M1, and the plots of the mean value variation with respect to ns are more separated.

6.1   Comparison between probabilistic models

In Figures 5 and 6, the PDF and CDF of the buckling load ($f[P_{cr}]$ and $F[P_{cr}]$), for each probabilistic model, are presented for the number of independent MCS that gives a prescribed accuracy. The differences between the PDFs and CDFs obtained with M1 and M2 can be observed. Both models show an increase of the standard deviation with the increment of d.

The $F[P_{cr}]$ in Figure 5 shows a particular point in which $P(P_{cr} \le P_0)$ is approximately equal for all the values of d. From this point towards the upper percentiles of the $F[P_{cr}]$ and for the same probability, the values of P_{cr} increase with the increment of d, and *viceversa* from this point to the lower percentiles of $F[P_{cr}]$. A homogeneous column presents the highest and the lowest values of buckling load in comparison with an inhomogeneous column, and also shows a larger variation or dispersion from the average or expected value of P_{cr}. In the PDF and CDF ($f[P_{cr}]$ and $F[P_{cr}]$) of M2, Figure 6, the difference of this model respect to M1 are shown. The PDF and CDF have a same initial point, in this region the columns have a larger amount of knots
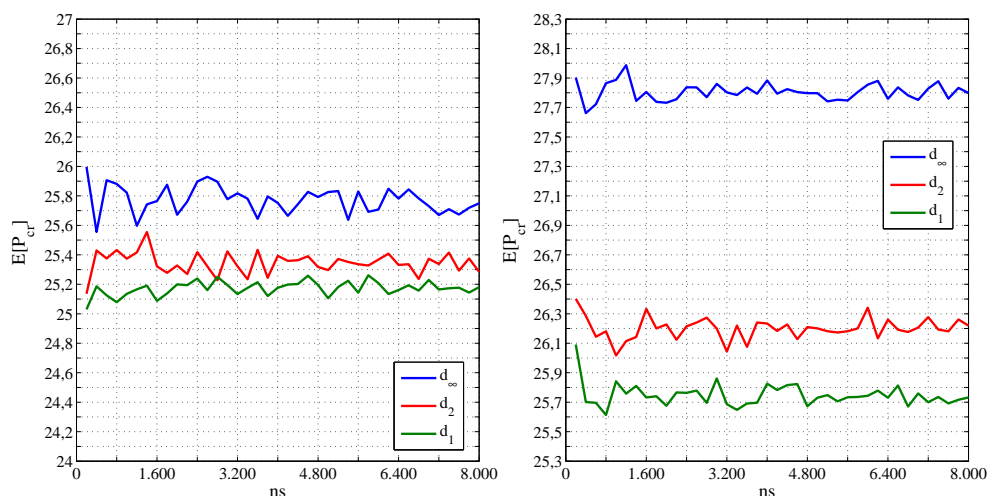
Figure 4: Convergence of $E[P_{cr}]$ obtained through the two models (M1 and M2) for different values of d.

and the lengthwise variation of the MOE in the sections without knots is not relevant. From this initial point towards the upper percentiles of the $F[P_{cr}]$ for the same probability, the values of P_{cr} increase with the increment of d. This behavior is similar to that shown in the upper percentiles of M1. One possible explanation of this result could be that the buckling load of columns with higher stiffness and lower number of defects are located in this region. In Figure 7 and Table 5 the results of the comparison between $F[P_{cr}]$ of the models for the same value of d are presented. As can be seen when d tends to zero, i.e. the MOE random field becomes a set of uncorrelated random variables in both models, the differences in the results between $F[P_{cr}]$ for M1 and M2 decrease.

In the first plot, d_∞ for both models, the differences in the lower percentiles can be explained due to the non-correlation of the MOE values in the sections with knots and to a lesser degree due to the PDF of the MOE in the sections without knots of the M2 because the columns in this zone have a considerable amount of defects. In the upper percentiles of $F[P_{cr}]$ the models become approximately similar, M2 generates columns with higher stiffness and lower number of defects and M1 generates columns with higher stiffness. Probabilistic models have show

	d_∞		d_2		d_1	
	M1	M2	M1	M2	M1	M2
$E[P_{cr}]$ (KN)	25.749	27.798	25.284	26.219	25.180	25.732
$\sigma[P_{cr}]$ (KN)	4.765	3.791	3.664	3.474	3.020	3.146

Table 5: Comparison of numerical results obtained with the probabilistic models for different values of d.

similar results for columns of superior quality, i.e. with a lower amount of defects in M2 and a higher stiffness in both models. At the same time M2 generates columns of lower quality with a higher buckling load than the M1. This difference between the models in the region of lower quality columns is reduced when d decreases and the components of the random field become less correlated.
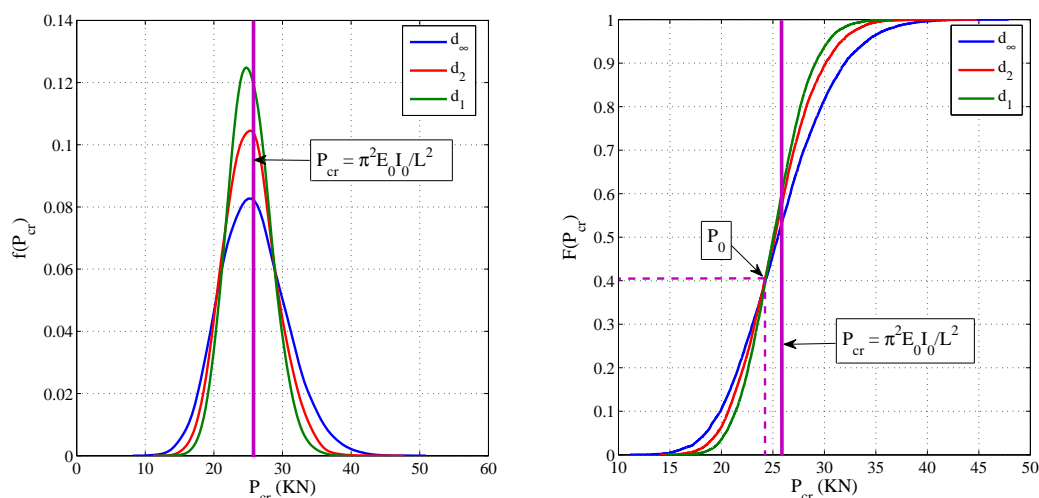
Figure 5: PDF and CDF of P_{cr} for different values of d, M1. $E_0 = 12.639$ GPa, $I_0 = 8.263$ x 10^{-7} m ^{4}, $P_{cr} = 25.768$ KN.

6.2   Influence of the random field I(x)

In this section, the influence of the random field $I(x)$ in P_{cr} is presented. To accomplish this in M2, the MOE assumes a deterministic constant value along the column. In Figure 8 the PDF and CDF of P_{cr} are shown. The value $E_0 I_0$ is the reference stiffness, corresponding to $E_0 = 15.889$ GPa and $I_0 = 8.263$ x 10^{-7} m^4. The buckling load associated with the reference parameters is $P_{cr} = 32.394$ KN. As can be observed, the range of the results is lower and the influence of the random field $I(x)$ is negligible with respect to the influence of the random field $E(x)$. From the figure can be observed that $P(P_{cr} \leq 31.5 KN) = 0.1$ and this represent 2.64 % of difference with respect to the reference buckling load. This value indicate the lower influence of $I(x)$ in the buckling load.

6.3   Comparison between Nataf transformation and non-Gaussian Karhunen-Loeve Expansion

In this section, the comparison between the results for M1 obtained with the random field of the MOE simulated by the Nataf transformation and the non-Gaussian Karhunen-Loeve Expansion (KLE) are presented and discussed.

In Figure 9, the first six eigenvalues and their corresponding eigenfunctions are shown for the adopted exponential correlation function and d_2. The solutions were presented in Ghanem and Spanos (1991) for an exponential covariance function.

The basis random variables ξ_i for the non-gaussian KLE are found with the method presented by Mulani et al. (2007), starting from the prescribed Gamma marginal PDF of the MOE presented in Table 3. The PDF of these basis random variables ξ_i (f_{nm}^*), for a Gamma marginal PDF of the random field, is the following:

$$f_{nm}^*(\xi \mid a_{nm}^*, b_{nm}^*, u) = \frac{1}{{b_{nm}^*}^{a_{nm}^*} \Gamma(a_{nm}^*)} (\xi - u)^{(a_{nm}^*-1)} e^{-\frac{(\xi-u)}{b_{nm}^*}} \qquad \xi \in [u, \infty) \qquad (34)$$

where $u = a_{nm}^* b_{nm}^*$, $a_{nm}^* = a$ and $b_{nm}^* = a^{-1/2}$ are the location, shape and scale parameters respectively (c.f. Table 3). The basis random variables ξ_i simulated from Eq. 34 fulfill with the requirements established by the Eq. 27.
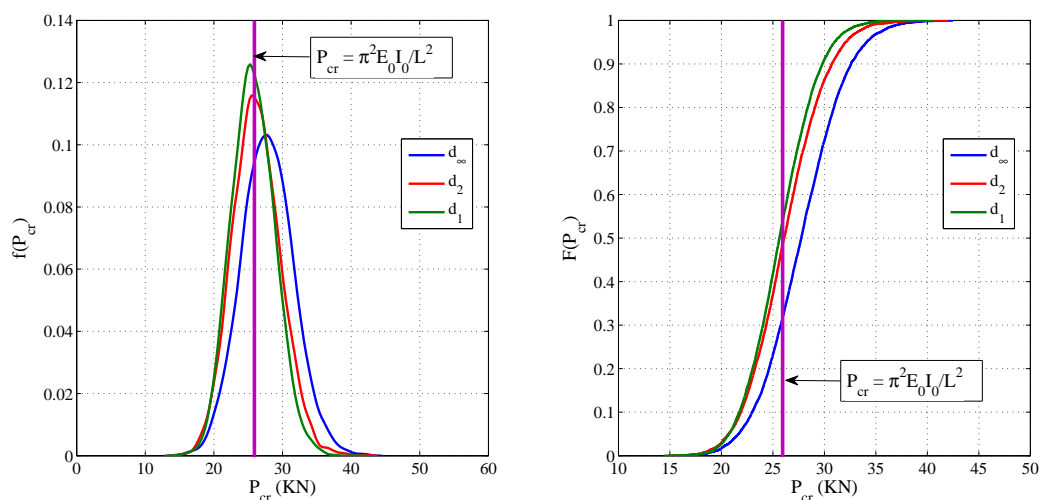
Figure 6: PDF and CDF of P_{cr} for different values of d, M2. $E_0 = 12.639$ GPa, $I_0 = 8.263$ x 10^{-7} m ^{4}, $P_{cr} =$ 25.768 KN.

In Figure 10 the comparison between the PDF and CDF of P_{cr} obtained for the random field simulated with the Nataf transformation and with the non-Gaussian KLE of order ten ($M = 10$) respectively is presented. It can be observed that the two approaches conduce to similar results for the two values of correlation length employed (d_1 and d_2). In Table 6 statistics values of the numerical results are presented. The similarity of the results can be observed for the mean value and standard deviation of P_{cr}. In Figure 11 the simulated marginal PDF of the MOE in one

	d_1		d_2	
	Nataf	KLE	Nataf	KLE
$E[P_{cr}]$ (KN)	25.180	25.252	25.284	25.373
$\sigma[P_{cr}]$ (KN)	3.020	3.140	3.664	3.779

Table 6: Comparison of numerical results obtained with the probabilistic models for different values of d.

point of the space through the two approaches are compared with the prescribed marginal PDF. It can be observed that the PDF obtained through the Nataf transformation fits better with the analytical one than the obtained through the KLE. This feature can be modified increasing the expansion order of the KLE. In Figure 12 some realizations of the MOE random field for both methods and different values of d are shown. In Figure 13 a comparison between the simulated and the prescribed covariance function is presented. When the expansion order increases, the obtained covariance function fits best with the prescribed one. Also the simulated covariance function obtained through the Nataf transformation presents higher values than the prescribed one for a lower distance between the spatial points.

7 CONCLUSIONS

The buckling load in structural size sawn *Eucalyptus grandis* columns with uncertain material properties was studied. The stochastic analysis allows obtaining more information of the behavior of the structural component.

The characterization and the study of the mechanical properties that are considered in the buckling problem were addressed. The statistical study of the timber knots dimensional param-
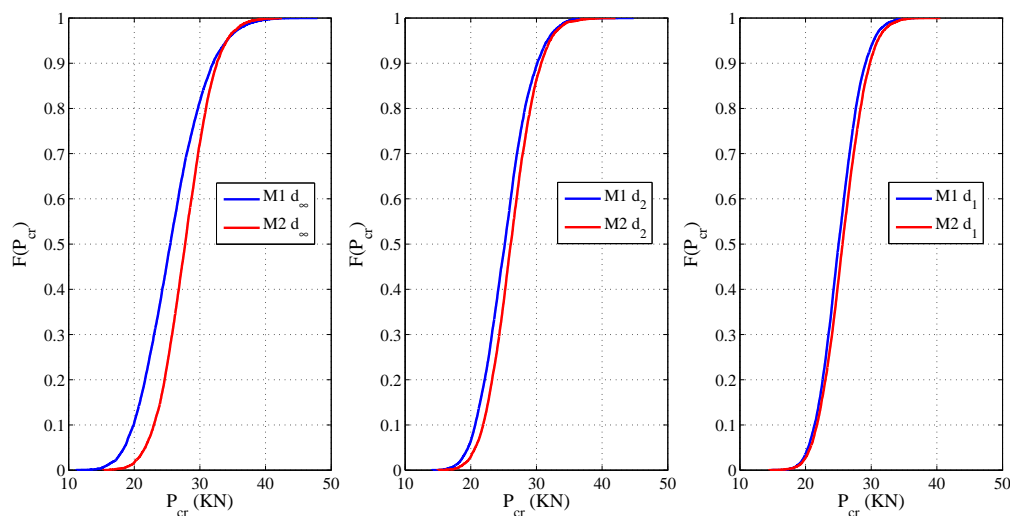
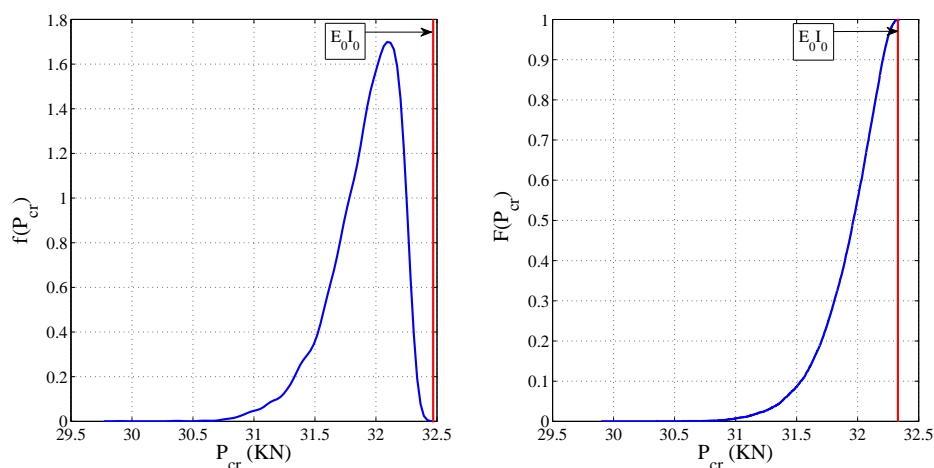Figure 7: Comparison of $F[P_{cr}]$, for M1, M2 and different values of d.

Figure 8: PDF and CDF of P_{cr} considering only the random field $I(x)$, M2.

eters and a method to simulated them and consider its influence in the random field $I(x)$ was presented. The influence of the timber knots in the response is frequently disregarded. In the present study, its consideration derives in an improved representation of sawn timber structures. The statistical study of the global MOE of this timber specie was presented. The traditional criterion to employ a normal PDF for the mechanical properties was addressed showing that the PDF that best fits the experimental results is the Gamma PDF. The Nataf transformation and the non-Gaussian Karhunen-Loeve Expansion are presented in order to simulate the MOE random field $E(x)$.

Two probabilistic models were presented. The first is a traditional timber model that only considers the lengthwise variability of the MOE (M1). The second one is an alternative model of the lengthwise variability of the MOE (M2) that starts from the weak-zone representation. This model introduces the presence of knots in the sectional parameters, the length of the weak zone in a different way than the weak-zone model, the choice of the parameters of the marginal PDF of the MOE depending of the section knot ratio (K) and the lengthwise variability of the
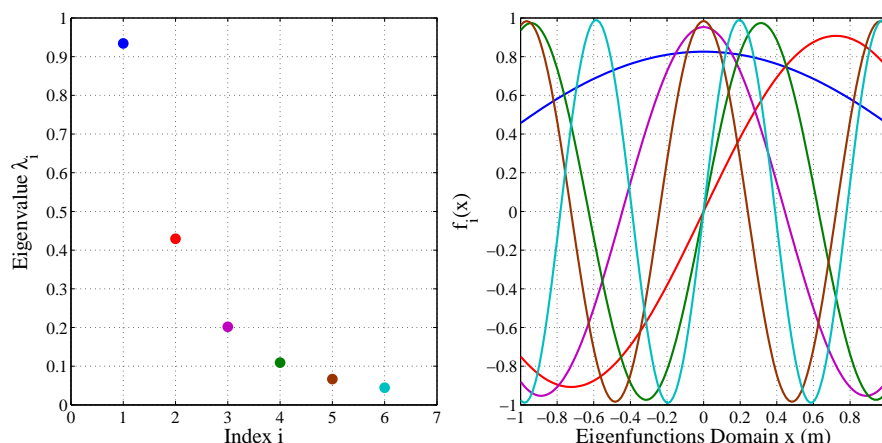
Figure 9: First six eigenvalues and eigenfunctions of the exponential covariance function for d_2.
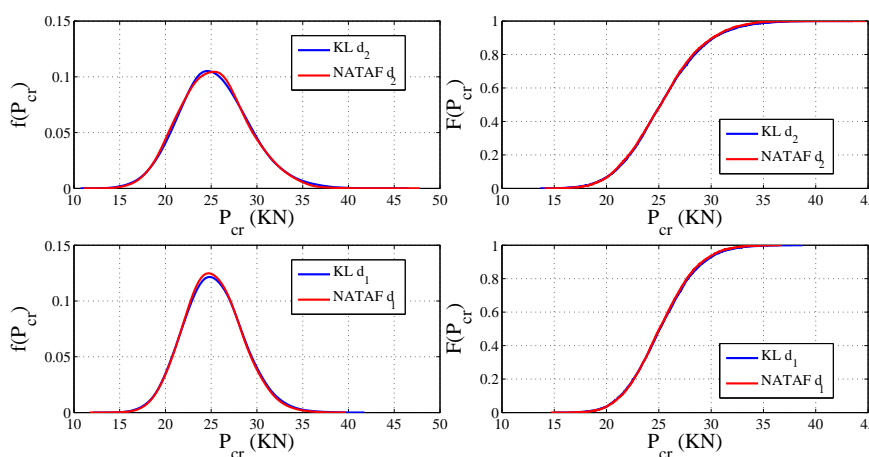

Figure 10: Comparison between the PDF and CDF of P_{cr} for the random field of the MOE simulated through the Nataf transformation and the Karhunen-Loeve Expansion.

MOE in the free of knots sections. The PDF of the buckling load of the timber column, with uncertain properties, was obtained with numerical simulations for both probabilistic models. They showed similar results for columns of superior quality, i.e. with a lower amount of defects in M2 and a higher stiffness in both models. At the same time, M2 produces columns of lower quality with a higher buckling load than the M1. This difference between the models in the region of lower quality columns is reduced when the correlation length d decreases and the components of the random field become less correlated.

The influence of the random field $I(x)$ in the buckling load is negligible with respect to the influence of the random field $E(x)$. The most important feature introduced by the knots presence is the lengthwise variability of the MOE.

For the probabilistic model M1, the comparison among the results obtained with the Nataf transformation and the non-Gaussian KLE was presented. In the latter the PDF of the basis random variables was presented. The PDF and CDF of the buckling load obtained with both approaches are similar. The properties and characteristic of the simulated random field $E(x)$ are compared and presented. The KLE reproduces more accurately the properties of the random
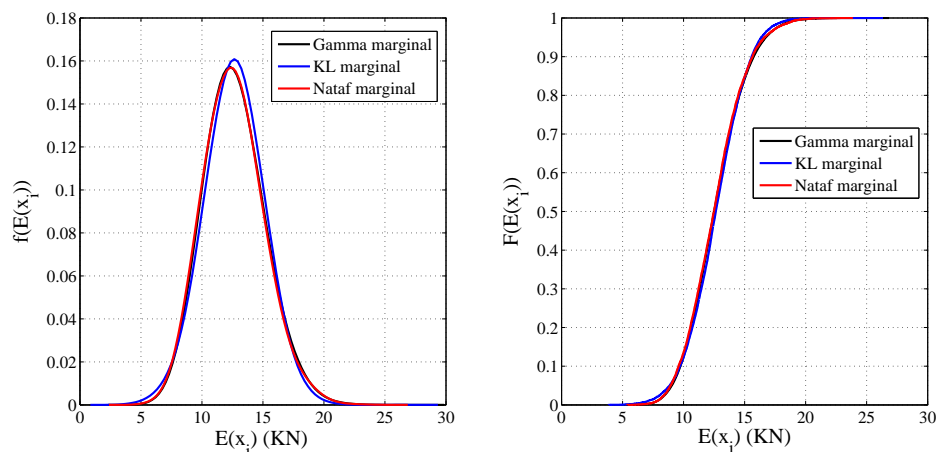
Figure 11: Comparison between the simulated and the prescribed marginal PDF and CDF of the MOE.
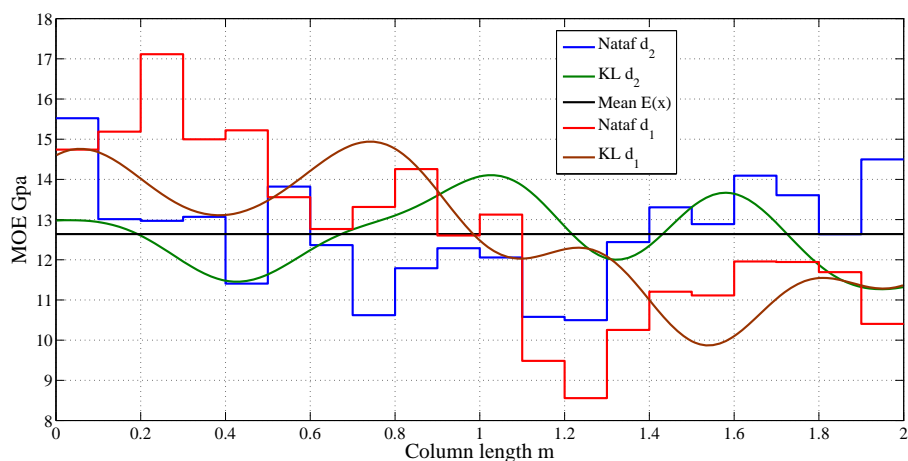

Figure 12: Realizations of the MOE random field.

field than the Nataf transformation. But the differences between the prescribed and the simulated properties of the random field for both approaches are small. In favor of the non-Gaussian KLE this difference decreases with the increment of the expansion order.

The stochastic models presented in this paper constitute a more realistic material approach, feasible to be applied to reliability studies of structural components made of $Eucalyptus\ grandis$ timber.

8 ACKNOWLEDGEMENTS

REFERENCES

Bathe K.J. *Finite element procedures*, volume 1. Prentice hall Englewood Cliffs, 1996.

Benjamin R.J. and Cornell C.A. *Probability, Statistics and Decision for Civil Engineers*. McGraw-Hill, 1970.

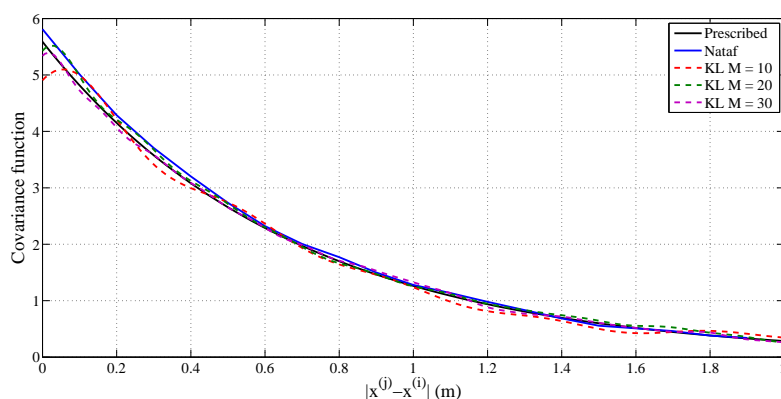Czmoch I. *Influence of structural timber variability on reliability and damage tolerance of*

Figure 13: Comparison between the simulated and the prescribed covariance function.

timber beams. Ph.D. thesis, Luleå tekniska universitet, 1998.

Der Kiureghian A. and Ke J.B. The stochastic finite element method in structural reliability. *Probabilistic Engineering Mechanics*, 3(2):83–91, 1988.

Der Kiureghian A. and Liu P.L. Structural reliability under incomplete probability information. *Journal of Engineering Mechanics*, 112:85–104, 1986.

Ditlevsen O. and Madsen H.O. *Structural reliability methods*, volume 178. Citeseer, 1996.

Escalante M.R., Rougier V.C., Sampaio R., and Rosales M.B. Buckling of wood columns with uncertain properties. *Mecánica Computacional, Volume XXXI. Number 14. Uncertainty and Stochastic Modeling*, pages 2735–2744, 2012.

Ghanem R.G. and Spanos P.D. *Stochastic finite elements: a spectral approach*, volume 41. Springer, 1991.

INTA. *Manual para productores de eucaliptos de la Mesopotamia Argentina*. INTA, 1995.

IRAM 9662-2. *Madera laminada encolada estructural. Clasificación visual de las tablas por resistencia. Parte 1 Tablas de Eucalyptus grandis*, 2006.

Isaksson T. *Modeling the Variability of Bending Strength in Structural Timber: Length and Load Configuration Effects*. División of the Structural Engineering, Lund University, 1999.

Köhler J. *Reliability of timber structures*. 301. vdf Hochschulverlag AG, 2007.

Köhler J., Sørensen J.D., and Faber M.H. Probabilistic modeling of timber structures. *Structural safety*, 29(4):255–267, 2007.

Melchers R.E. *Structural reliability analysis and prediction*. John Wiley New York, 1999.

Mulani S., Kapania R., and Walters R. Karhunen-loeve expansion of non-gaussian random process. 48 th AJAA/ASME/ASCE/AHS/ASC Structures, Structural Dynamics and Materials Conference, 2007.

Piter J. *Clasificación por resistencia de la madera aserrada como material estructural. Desarrollo de un método para el Eucalyptus grandis de Argentina*. Ph.D. thesis, Tesis Doctoral). 206 p. Universidad Nacional de la Plata, 2003.

Piter J. Visual survey of $Eucalyptus\ grandis$ sawn beams. *Personal Communication*, 2013.

Rubinstein R.Y. *Simulation and the Monte Carlo method*. John Wiley and Sons, Inc., 1981.

Shannon C. A mathematical theory of communication. *The Bell technical journal*, 27:379–423, 1948.

UNE-EN408. Estructuras de madera. Madera aserrada y madera laminada encolada para uso estructural. Determinación de algunas propiedades físicas y mecánicas. *Estructuras de Madera, Editado por AENOR-Asociación Española de Normalización y Certificación, Madrid*, 1995.